X-Ray Interferometry with Multicrystal Components Using Intensity Correlation

K. Tamasaku,[1] M. Yabashi,[2] and T. Ishikawa[1,2]
[1]*SPring-8/RIKEN, Mikazuki, Hyogo 679-5148, Japan*
[2]*SPring-8/JASRI, Mikazuki, Hyogo 679-5198, Japan*
(Received 12 June 2001; published 14 January 2002)

A theoretical relation between intensity correlation and interference was experimentally verified for the case of a large-separation skew-symmetric bicrystal interferometer. The intensity correlation was enhanced in the angular range where the interference fringes were clearly observed. An application investigating the interference condition of the interferometer is presented using the intensity-correlation technique.

DOI: 10.1103/PhysRevLett.88.044801 PACS numbers: 41.50.+h, 42.25.Hz

Interferometry is one of the most basic and powerful methods to perform spectroscopy and metrology with electromagnetic waves. Introduction of a crystal interferometer to the hard x-ray region by Bonse and Hart [1] facilitated unique applications utilizing its shortness of wavelength, such as studying defects in nearly perfect crystals, measurement of lattice parameters, and phase contrast imaging [2]. On the other hand, because of the short wavelength, x-ray crystal interferometers are widely believed to require nanometer stability. This has forced most researchers to consider only a monolithic arrangement where the splitter, mirror, and analyzer are built in a single block of highly perfect silicon crystal. However, some attempts at constructing multicrystal interferometers have succeeded with symmetric triple-Laue type (LLL) [3] and skew-symmetric LLL interferometers [4] using elaborate stabilization of separate blocks as if they were made of a single block. Separation of the crystals allows scanning of a single component of the interferometer, such as the analyzer for precise measurements of lattice spacing [5] and anomalous dispersion [6]. To build an interferometer from separate crystal blocks the interference area was extended beyond that obtained from a single block for phase contrast imaging over a wide area [7,8].

Previous separate-crystal interferometry devices have limitations. The separate blocks were mounted on a common rotational stage to overcome the stringent stability requirements. But a common stage is not compatible with an increased separation between blocks, where variable optics and samples might be inserted. A large-separation interferometer may be able to detect the redshift of x rays due to a gravitational field [9]. The combination of separate, stabilized blocks with conventional static interferometry, where images of interference fringes are taken or interference intensity oscillation is measured, is suitable for phase sensitive applications [5,6,8] rather than visibility sensitive applications. Visibility measured by the conventional static method is subject to degradation caused by residual instability. Such degradation is harmful to the visibility sensitive applications, such as coherence measurements by Young and Michelson-type interferometers, which may compare visibility measured under different conditions. New interferometric methods to determine visibility without needing to stabilize the interferometer would open a wider field of applications for multicrystal-component x-ray interferometers.

Recently, using a monolithic interferometer, we have shown that the intensity correlation between the reflected and the transmitted beams from an interferometer is related directly to the visibility of the interference fringes when the phases of two interfering beams fluctuate [10]. This implies that nanometer stability is not needed to perform x-ray interferometry with multicrystal interferometers. In this Letter we consider the intensity correlation in the output beam of a fluctuating multicrystal interferometer differently than in a previous study [10]; by concentrating on visibility and ignoring the effects of photon statistics. We apply the result to a large-separation skew-symmetric LLL bicrystal interferometer and clarify the interference condition. This is the first report of a "large separation" interferometer, where each crystal block is mounted on an independent rotational stage.

The intensity oscillation of the output beam from a multicrystal interferometer is written as

$$I = \langle I \rangle (1 + V \cos\phi), \tag{1}$$

where $\langle I \rangle$ is the average intensity and V is the visibility of the oscillation. ϕ is proportional to the relative angular or positional shift among the component blocks. When the output intensity is monitored simultaneously by two detectors giving output signals of I_1 and I_2 the time-averaged correlation is written as

$$\langle I_1 I_2 \rangle = \langle I_1 \rangle \langle I_2 \rangle \langle 1 + 2V \cos\phi + V^2 \cos^2\phi \rangle . \tag{2}$$

Here we ignore enhancement of the intensity correlation by the chaotic nature of the synchrotron radiation because the temporal coherence of the incident beam for a typical setup is much shorter than the pulse width of x rays [10–12]. When the interferometer is unstable and the phase variable ϕ scans a wide range during measurement, Eq. (2) becomes

$$\langle I_1 I_2 \rangle = \langle I_1 \rangle \langle I_2 \rangle (1 + V^2/2) . \tag{3}$$

Here we assume V is a slowly varying quantity of ϕ. Thus, the visibility of the interference is measured directly

through a coincidence rate $P_{12} = \langle I_1 I_2 \rangle / \langle I_1 \rangle \langle I_2 \rangle$. The upper and lower envelopes of the intensity oscillation are given by $\langle I_1 \rangle (1 \pm V)$. When two detectors monitor different locations in the beam section or different branches of the output beams the coincidence rate includes information on the visibilities of the monitored oscillations and their phase difference.

For skew-symmetric bicrystal interferometers the intensity of the output beam oscillates when one of the blocks rotates relative to the other within the scattering plane. The angular period of oscillation, Φ, is related to the relative shift between the standing wave created by two interfering beams and the diffracting netplanes of the analyzer [1], as $\Phi = d/(x + t)$ where d, x, and t are the lattice spacing, the splitter-to-mirror (mirror-to-analyzer) distance, and the thickness of the blades, respectively [4]. Φ falls within the order of a nanoradian, so that it is probable that subnanoradian resolution and stability are required for the conventional static interferometric method. A stability on the order of 10^{-7} radian and/or meter can be achieved by commercially available rotation and translation stages, but not down to 10^{-10} because of thermal drift and mechanical vibration. The assumption made to obtain Eq. (3) is satisfied with use of these stages for a multicrystal interferometer.

We chose a skew-symmetric bicrystal interferometer to verify the theory presented above and to investigate interference conditions for future applications [9]. Figure 1 shows schematically the experimental setup at BL29XUL in the SPring-8 [13]. The experiment was performed at a wavelength of 0.663 Å. First two crystals acted as a beam expander to enlarge the beam vertically for imaging measurement. The expander consisted of asymmetric diffraction with an asymmetric angle of $\alpha = 9.00°$ and symmetric diffraction with Si 220 crystals. We prepared two blocks of the skew-symmetric bicrystal interferometer

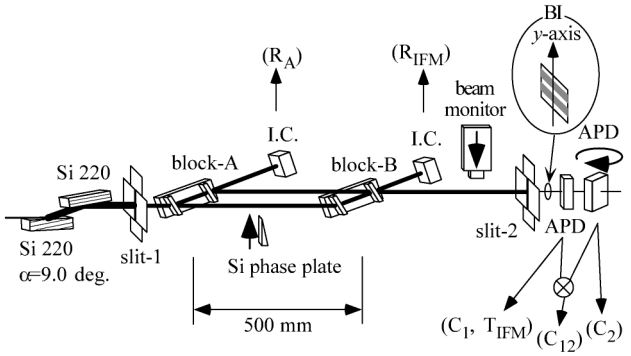

FIG. 1. Schematic side view of the experimental setup for coincidence measurement. Two crystal blocks of the interferometer, A and B, were mounted on individual precision goniometers, which were separated by 500 mm. The beam monitor and the Si phase plate were inserted into the beam path when the beam images were taken. IC: ionization chamber; APD: avalanche photodiode; BI: an enlarged image of the beam section with interference fringes and y coordinate used to obtain Eq. (5) (see text).

with 220 diffraction planes from a single Si block. The interferometer had $t = 3$ mm blade thickness and a splitter-to-mirror (mirror-to-analyzer) distance of $x = 50$ mm. The angular period of the oscillation was estimated to be $\Phi = 3.6$ nrad. Each block of the interferometer, A and B, was mounted independently on a separate precision goniometer [13,14]. The separation between the two blocks was set at 500 mm. To adjust the tilt angle between the blocks, the second goniometer was mounted on a tilt stage. The incident angles on the blocks, θ_A and θ_B, were measured as deviation angles from the peaks of the reflected intensities, R_A and R_{IFM}, respectively.

To measure the intensity correlation, we used a coincidence technique. Two semitransparent silicon avalanche photodiodes (APD) were set in tandem into the transmitted beam from the interferometer, T_{IFM}. The second APD was inclined to increase the effective thickness of the device to compensate for the absorption of the first APD. To avoid smearing the correlation the detection area should not extend beyond the intrinsic Moiré fringes [1]. A slit with an aperture of 300(H) $\times$ 150(V) μm^2 was set in front of the APD. The aperture was much smaller than the intrinsic fringe spacing, approximately 4 mm, after alignment of the tilt between the two blocks [15]. The output signal of the APD was gated by a signal at a frequency of 10 MHz and 40 ns duration, which was chosen to fit the bunch structure of the storage ring and to be much faster than the time scale of the intensity fluctuation caused by mechanical vibration. The gated signal was converted to a pulse 44 ns wide to avoid generating more than two signals within a single gate. The measured count rate of the converted pulses was less than 3×10^5 cps, which was sufficiently smaller than the number of gates per unit time, $N = 1 \times 10^7$, and did not cause saturation. The signals from the APD were counted as C_1 and C_2, and the coincidence signal as C_{12}, after a coincidence unit.

First, the θ_B dependence of the coincidence rate was measured from $-1.75''$ to $0.75''$ in $0.025''$ steps, whereas θ_A was fixed at $-0.5''$. The integration time was $T = 0.5$ s for each point. Since the intensity was measured by photon counting, the coincidence rate, P_{12}, is given by

$$P_{12} = \frac{N}{T} \frac{C_{12}}{C_1 C_2}. \tag{4}$$

During the experiment the storage ring was operated in the partially filled bunch mode, i.e., 1760 of 2436 bunches were filled. The coincidence rate is plotted in Fig. 2 using a normalization factor of $1760N/2436T = 1.44 \times 10^7$ s^{-1} together with the reflected (R_{IFM}) and the transmitted (T_{IFM}) intensities from the interferometer. A visibility of 97% was deduced from the maximum value of $P_{12} = 1.47$ at $\theta_B = -0.5''$.

The coincidence rate was enhanced only within an angular range of $0.15''$ around $\theta_A = \theta_B = -0.5''$, whereas the widths of diffraction, T_{IFM} and R_{IFM}, were about $1''$. The visibility of the transmitted beam expected from

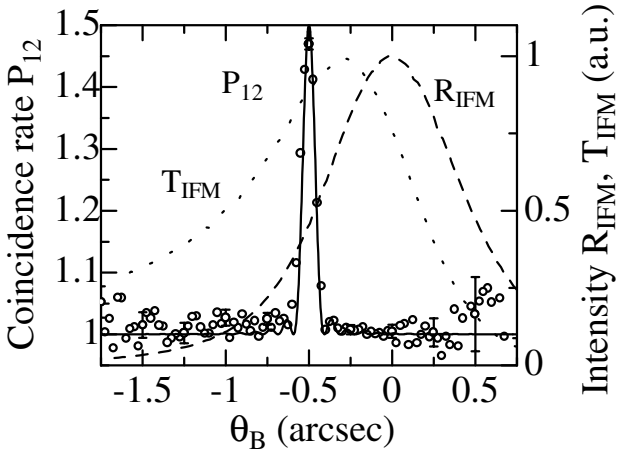

FIG. 2. The θ_B dependence of the coincidence rate, P_{12} (open circles), the transmitted intensity T_{IFM} (dotted line), and the reflected intensity R_{IFM} (dashed line) at $\theta_A = 0.5''$. The vertical bar on P_{12} indicates the statistical error. The solid line was calculated P_{12} by Eq. (5).

a simple picture is given as $V = 2R_1R_2\sqrt{T_1T_2}/(R_1^2T_2 + T_1R_2^2)$, where $T_{1,2}$ and $R_{1,2}$ are, respectively, the reflectivity and transmissivity of Si 220 diffraction in the Laue case at $\theta_{A,B}$. P_{12} should be enhanced in a wider range than the observation, standing on the simple picture. The difference can be explained as follows. When one of the blocks was rotated slightly within the scattering plane by $\Delta\theta$ from exactly parallel, the period of a standing wave imposed upon the analyzer was $\pi/(k_\perp + \Delta\theta k_\parallel)$, which did not match the netplanes of the analyzer. Here, $k_\parallel$ and $k_\perp$ are the parallel and perpendicular components of the x-ray wave number to the netplane. This mismatch will cause a kind of Moiré fringe parallel to the netplane with a period of $\Lambda = \pi/\Delta\theta k_\parallel$, similar to the situation of thermally induced lattice dilation [16]. Since the detection area is finite, the phase of V in Eq. (1) is no longer constant over the area. Equation (1) can be modified as $I = \langle I\rangle[1 + V\cos(2\pi y/\Lambda + \phi)]$, where y denotes the position in the detection area along the perpendicular direction to the Moiré fringes (Fig. 1). Integrating Eq. (2) over the detection area, Eq. (3) is rewritten as

$$P_{12} = 1 + \frac{V^2}{2}\left[\frac{\sin(\pi w/\Lambda)}{\pi w/\Lambda}\right]^2, \qquad (5)$$

where w is the width of the area perpendicular to the Moiré fringes. P_{12} calculated by Eq. (5) with a slit size of $w = 150\ \mu$m, $V = 1$, and $\Delta\theta = \theta_B + 0.5''$ is plotted in Fig. 2. The experimental observation is explained well by Eq. (5).

To confirm that interference took place where P_{12} was enhanced, the transmitted beam images from the interferometer were recorded by a CCD-based beam monitor (Hamamatsu Photonics, AA-20MOD). A Si wedge with an apex angle of 3° and with its edge horizontal was inserted into one branch of the interferometer as a phase shifter and produced dense fringes in the field of view for visibility measurement (Fig. 1). The exposure time was as short as 2 ms to reduce smearing of the fringes due to angular fluctuation of the interferometer. Figure 3 shows the correspondence of the angular range, where the interference fringes were observed, with regions where P_{12} was enhanced. However, the visibilities estimated from the images were smaller than those expected from P_{12}, probably due to differences in integration time.

Since visibility was directly related to P_{12}, interference was easily investigated for any possible freedom of motion of a multicrystal interferometer. Figure 4 shows a two-dimensional map of the measured P_{12} within a rectangular region of $-2.0'' < \theta_{A,B} < 1.0''$. This survey clearly demonstrated that a narrow angular region around $\theta_A = \theta_B$ was usable for interferometry. The width of the region was found to be nearly constant along the line, as expected from Eq. (5). When two blocks were kept parallel, i.e., $\theta_A = \theta_B$, they worked as an interferometer over the considerable angular range of diffraction (see the inset in Fig. 4). The earlier report of visibility by Becker and Bonse [4] corresponds to the constant θ_A line in the map, and that by Momose *et al.* corresponds to the $\theta_A = \theta_B$ line [8]. Both observations are qualitatively consistent with the present result, although the wavelength and the parameters of the interferometer are different.

For a quantitative analysis of visibility, one should be careful of the normalization process. If the incoming intensity fluctuates, the intensity correlation will be enhanced even when $V = 0$, in the same manner as Eqs. (1)–(3). For example, unequal bunch numbers in each gate and/or nonuniform stored current in each bunch will cause intensity modulation. These can be reasons why the base line of P_{12} in Fig. 2 is slightly greater than unity. Precise analysis of the visibility might require estimating fluctuation of the incoming beam intensity, which is measured by intensity correlation without the interferometer.

In summary, we have derived a relation between the visibility and intensity correlation, and demonstrated validity of the theory using a large-separation bicrystal interferometer. The intensity correlation technique, combined with a fluctuating multicrystal interferometer, was found to be

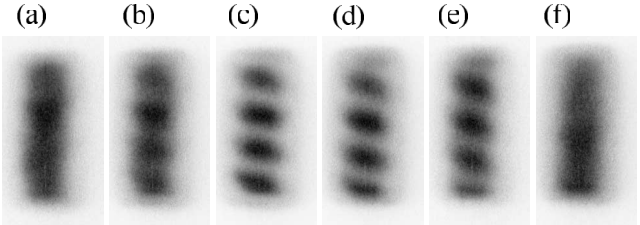

FIG. 3. Transmitted beam images taken by the beam monitor around the peak of P_{12} in Fig. 2. The vertical beam size was 5 mm. θ_B and V were (a) $-0.60''$ and 0%; (b) $-0.55''$ and 18%; (c) $-0.50''$ and 42%; (d) $-0.45''$ and 33%; (e) $-0.40''$ and 20%; (f) $-0.35''$ and 0%.

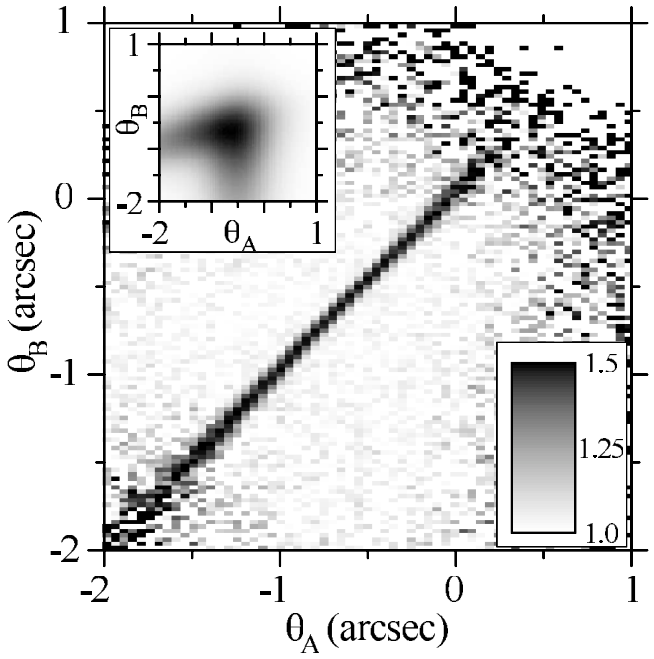

FIG. 4. Map of the coincidence rate P_{12} and the transmitted intensity T_{IFM} (inset). The regions around $\theta_{\mathrm{A,B}} = -2.0''$ and $1.0''$ have large error bars due to poor statistics.

an easy and direct measure of visibility without stabilizing the interferometer, scanning a phase plate, or taking an image of the interference fringes. Since the intensity correlation was measured instantaneously, the visibility was free from degradation due to instability, which is unavoidable for conventional static interferometry. The intensity correlation technique gave a firm means to compare the visibility measured under different conditions, such as at different angles or positions of the one component of the interferometer. As demonstrated in Fig. 4, this was quite useful to investigate the interference phenomena of multicrystal interferometers and to find the best conditions for interference.

The present technique will serve for a Michelson-type interferometer in the x-ray region. Currently available Michelson interferometers have scanning ranges for a path difference on the order of micrometers [17] or millimeters [18]. A large path difference, on the order of hundreds of millimeters to even tens of meters, is achievable using completely separate crystals. Such an interferometer combined with the Fourier transform method is useful in ultrahigh-resolution spectroscopy. The energy resolution, which is proportional to the wavelength and the inverse of path difference, can be very high owing to the short wavelength of x rays, e.g., a path difference of 1 m at 1 Å corresponds to an energy resolution of 10^{-10}. One possible application may be Mössbauer spectroscopy with x rays which gives important information about hyperfine splitting of nuclei [19]. It might be difficult to observe quantum beats by time domain measurement [20] for materials with larger hyperfine splitting (higher beat frequency) and/or larger line width (faster decay rate), because of the limited time resolution of detectors. A path difference of 30 mm corresponds to a time resolution of about 0.1 ns, which is inaccessible with currently available fast detectors. The spectrum of the multiplet could be resolved by Fourier transform x-ray spectroscopy.

We are grateful to Dr. K. Inoue for the loan of a fast shutter CCD camera, and Dr. A. Q. R. Baron for preparation of the APD.

[1] U. Bonse and M. Hart, Appl. Phys. Lett. **6**, 155 (1965).
[2] U. Bonse and W. Graeff, in *X-Ray Optics,* edited by H.-J. Queisser (Springer-Verlag, Berlin, 1977), Chap. 4, and references therein.
[3] U. Bonse and E. te Kaat, Z. Phys. **214**, 16 (1968).
[4] P. Becker and U. Bonse, J. Appl. Crystallogr. **7**, 593 (1974).
[5] R. Deslattes and A. Henins, Phys. Rev. Lett. **16**, 972 (1973).
[6] M. Hart and D. P. Siddons, Proc. R. Soc. London A **376**, 465 (1981).
[7] A. Momose, A. Yoneyama, and K. Hirano, J. Synchrotron Radiat. **4**, 311 (1997).
[8] A. Momose, T. Takeda, Y. Itai, A. Yoneyama, and K. Hirano, J. Synchrotron Radiat. **5**, 309 (1998).
[9] T. Ishikawa *et al.,* Proc. SPIE Int. Soc. Opt. Eng. **4145**, 1 (2000).
[10] M. Yabashi, K. Tamasaku, and T. Ishikawa, Jpn. J. Appl. Phys. **40**, L646 (2001).
[11] E. Ikonen, Phys. Rev. Lett. **68**, 2759 (1992).
[12] M. Yabashi, K. Tamasaku, and T. Ishikawa, Phys. Rev. Lett. **87**, 140801 (2001).
[13] K. Tamasaku *et al.,* Nucl. Instrum. Methods Phys. Res., Sect. A **467–468**, 686 (2001).
[14] T. Ishikawa *et al.,* Rev. Sci. Instrum. **63**, 1015 (1992).
[15] The tilt between two blocks was adjusted by minimizing the split width of the transmitted beams on the beam monitor, where the horizontal aperture of the slit 1 was set to 20 μm.
[16] U. Bonse and M. Hart, Z. Phys. **190**, 455 (1966).
[17] A. Appel and U. Bonse, Phys. Rev. Lett. **67**, 1673 (1991).
[18] K. Fezzaa and W.-K. Lee, J. Appl. Crystallogr. **34**, 166 (2001).
[19] For a recent review, see Special issue on *Nuclear Resonant Scattering of Synchrotron Radiation Part I,* edited by E. Gerdau and H. de Waard [Hyperfine Interact. **123/124** (1999); **125** (2000)].
[20] E. Gerdau, R. Rüffer, R. Hollatz, and J. P. Hannon, Phys. Rev. Lett. **57**, 1141 (1986).